

Contents lists available at ScienceDirect

Journal of Non-Newtonian Fluid Mechanics

journal homepage: www.elsevier.com/locate/jnnfm



Check for updates

The importance of initial extension rate on elasto-capillary thinning of dilute polymer solutions

Ann Aisling, Renee Saraka, Nicolas J. Alvarez *

Department of Chemical and Biological Engineering, Drexel University, Philadelphia, 19104, PA, USA

ARTICLE INFO

Keywords: Capillary breakup rheometry Elasto-capillary thinning Chain stretch Stress relaxation Relaxation time FENE Polymer physics CaBER

ABSTRACT

This work focuses on inferring the molecular state of the polymer chain required to induce stress relaxation and the accurate measure of the polymer's longest relaxation time in uniaxial stretching of dilute polymer solutions. This work is facilitated by the discovery that constant velocity applied at early times leads to initial constant extension rate before reaching the Rayleigh-Plateau instability. Such constant rate experiments are used to correlate initial stretching kinematics with the thinning dynamics in the final thinning regime. We show that there is a minimum initial strain-rate required to induce rate independent elastic effects, and measure the longest relaxation time of the material. Below the minimum extension rate, insufficient stretching of the chain is observed before capillary instability, such that the polymer stress is comparable to the capillary stress at long times and stress relaxation is not achieved. Above the minimum strain-rate, the chain reaches a critical stretch before instability, such that during the unstable filament thinning the polymer stress is significantly larger than the capillary stress and rate-independent stress relaxation is observed. Using a single relaxation mode FENE model, we show that the minimum strain rate leads to a required initial stretch of the chain before reaching the Rayleigh-Plateau limit. These results indicate that the chain conformation before entering the Rayleigh Instability Regime, and the stretching induced during the instability, determines the elastic behavior of the filament. Lastly, this work introduces a characteristic dimensionless group, called the stretchability factor, that can be used to quantitatively compare different materials based on the overall material deformation/kinematic behavior, not just the relaxation time. Overall, these results demonstrate a useful methodology to study the stretching of dilute solutions using a constant velocity stretching scheme.

1. Introduction

A long standing problem in the literature is the characterization of dilute polymer solutions in extensional flow. Due to the influence of capillary and gravitational forces, it is very difficult to independently measure the extensional stress of these materials. Furthermore, the relaxation time of these materials are too fast (<100 ms) to actively control the rate of deformation. The most successful experimental methods restrict themselves to measuring the relaxation time of the material, e.g. CaBER [1-6], drop on a substrate (DoS) [7-14], RoJER [15-17], and pulsed surface acoustic wave on a drop [SAW] [18]. For example, the capillary breakup rheometer, known as the CaBER, is designed to induce large elastic stresses at early time, such that the rate of thinning, proportional to the relaxation time of the material can be measured at later times. Such methods are better classified as an indexer rather than a rheometer since they do not actively control the deformation or stress. Since many of these apparatuses have different acronyms and variations in methodologies, it may not be obvious to the reader that almost all of them work on the same filament thinning principles. These techniques utilize initial uniaxial deformation to induce elastic stress in the material and measure the decrease in diameter with time. Initially the stress state of the material is imposed (not controlled) by the rate of motion of two fractions of the material stretched away from each other, henceforth referred to as *active stretching*. At some prescribed time, the bulk stretching is stopped and the stress state imposed on the material is controlled by interfacial stresses, henceforth referred to as *passive stretching*. There are two regimes of passive stretching, an early stage whereby the filament thins due to the Rayleigh–Plateau instability, and a late stage thinning whereby the filament diameter decays depending on the relative magnitudes of elastic stresses and capillary stresses.

In all techniques, the decay rate of the filament diameter during late stage passive stretching is used to determine a material relaxation time following the theory of Entov and Hinch, whereby the rate of thinning is inversely proportional to the longest relaxation time of the polymer chain at sufficiently long time [19]. It is important to note that the

E-mail address: alvarez@drexel.edu (N.J. Alvarez).

^{*} Corresponding author.

analysis of Entov and Hinch is based on no pre-stretching history of the material. The analysis yields the longest relaxation time only when the chain is sufficiently stretched that the longest relaxation mode of the chain dominates the stress and all faster relaxation modes have sufficiently relaxed. More specifically, Entov and Hinch show that the measured rate of thinning in their Fig. 4 only corresponds to the longest relaxation mode when the elastic stress in their Fig. 7 is dominated by this mode [19]. Unfortunately, in real experiments it is unclear which relaxation time is being measured when considering the analysis of Entov and Hinch. By the authors' own admission, the rate of thinning of the filament diameter in the late stage passive stretching regime depends on the spectrum of relaxation times. Furthermore, the state of the chain prior to entering the late stage passive stretching regime strongly impacts the rate of thinning of the filament diameter. Thus, it is unclear the role of pre-stretching on the measured rate of thinning in the late stage passive stretching regime, and whether more chain stretch in the active regime would lead to a clearer measurement of the longest relaxation time.

The major difference between the above mentioned CaBER type techniques is the method of active stretching. In the case of CaBER, a typical active stretching method employed is known as slow retraction [20], whereby initial plate separation velocities in the range of 0.005-2 mm/s are used to avoid later stage inertial effects [6,21]. Other methods, such as ROJER apply a significant active stretching rate prior to passive stretching. In a 2018 experimental study, the same material was compared in ROJER and CaBER, and the two methods resulted in different characteristic relaxation times determined from the analysis of Entov and Hinch [15]. The authors suggested that the issue between measurement techniques could be solved by applying different exponential scaling factors. However, the fact that different techniques have led to different measurements of relaxation time suggests that the initial active stretching rate does play an important role. The disagreement between ROJER and CaBER is also inline with the argument that poor control of material history is a key source of measurement variation and disagreement between experiment and theory [22]. Thus, there is a standing question whether the active stretching regime plays any role in the later stage elastic passive stretching regime. Unfortunately, this question cannot be answered by literature data as it is not customary to report the entire kinematic history of the stretching experiments, and typically only the passive stretching regime is reported. In this work, we show that slow retraction does not lead to a material relaxation time, but rather a timescale that depends on the rate of slow-retraction, suggesting that a different experimental protocol is needed to ensure an accurate measure of the longest relaxation time of the material.

We use a uniaxial extensional rheometer in constant velocity mode to demonstrate that there is a minimum initial extension rate during active stretching of a model polyethylene oxide solution that guarantees the measurement of the materials longest relaxation time from the late stage passive stretching regime. When these conditions are not met, a much faster relaxation time is measured, which is a function of initial active stretching rate. This method avoids the inertial issues of the CaBER by continuously moving the plates during passive stretching. We couple experimental data with a single mode FENE-P model to compare the elastic stress and capillary stress of the material as a function of time. We show that a rate independent relaxation time is only guaranteed when the rate of extension in the active stretching is above a critical Weissenberg number. Furthermore, our results show that there is a required minimum chain stretch, or minimum elastic stress, required at the end of active stretching to ensure the longest relaxation time is measured in the final thinning regime. Lastly, we introduce an additional parameter, referred to as the stretchability factor, that relates the overall behavior of the fluid in the applied kinematics. This new easy to measure parameter quantifies the geometric stretching of the material and is advantageous to state-of-the-art complex image analysis.

Table 1
List of variables used in the analysis of constant velocity extensional data.

Term	Equation
 Radial Hencky strain, ϵ_D	$\epsilon_D = 2 \ln \left(\frac{D_0}{D(t)} \right)$
Axial Hencky strain, ϵ_z	$\epsilon_z = \ln\left(\frac{H}{H_o}\right)$
Local strain rate, $\dot{e}_{D,\mathrm{local}}$	$\dot{\epsilon}_{D,\mathrm{local}} = \frac{d\epsilon_D}{dt}$
Steady state strain rate	$\dot{\epsilon}_{D,\mathrm{local}} = \mathrm{constant}$
Relaxation time	$\lambda = \frac{2}{(3\dot{\epsilon}_D)}$
Stretchability, S	$S = \left(\frac{\partial \epsilon_Z}{\partial \epsilon_D}\right)$
Stretchability Plateau	$\lim_{t\to\infty} S$

2. Materials and methods

Solutions of polyethylene oxide (Sigma Aldrich) with an average molecular weight of 4×10⁶ g/mol in water were prepared in concentrations of 10, 30, 60, 120, 240, 480, and 960 mg/L (wppm) by dissolving PEO in water, stirred, and allowed to sit for at least 24 h to ensure homogeneity [14]. Note that the overlap concentration for this Mw PEO has been previously measured to be 770 wppm [23]. The dissolved solutions were tested on an 8 mm parallel plate geometry attached to a Versatile Accurate Deformation Extensional Rheometer (VADER -Rheo Filament) at constant velocity separation of the top plate. The VADER software was changed to allow for a higher data collection rate (from 33 to 100 points/s) for these experiments. The maximum measured Hencky strain for the VADER is 8.76 based on the reported minimum measured diameter of $100 \mu m$. The stainless-steel plates were covered with tape (adhesive side not in contact with sample) to avoid sample slipping. Samples were loaded at constant volume (100 µL) onto the parallel plates using a micropipette. The top plate was lowered so that the diameter of the sample was approximately equal to that of the geometry plates (between 7.6-7.9 mm). The sample was scanned with the intrinsic laser micrometer to measure the initial diameter and shape. Uniform sample shape was visually confirmed by the user to ensure that no premature stretching occurred, and that the sample diameter was axisymmetric. The sample was allowed to relax in this state for a minimum of 30 s before stretching. The sample was stretched at constant velocity between 0.1-100 mm/s. Each concentration and velocity were repeated using three fresh sample loadings to ensure reproducibility. Furthermore each sample was tested three consecutive times (with sufficient time greater than 1 min for the sample to fully relax between runs) and the average of these measurements are reported. Two different researchers ran sample sets in an initial gauge analysis to identify, quantify, and manage sources of experimental variability and error — such as the length of time samples needed to relax, slip of material on plate, impact of bubbles, evaporation, and age of prepared solution (all of these matter). Minimum sample diameter and separation height of plates were collected as a function of time and analyzed to calculate strains and model stresses. Table 1 shows a list of all variables used to analyze and discuss the experimental data. Note that some of these are common in the extensional rheology literature; however we have introduced several new variables such as stretchability, S and stretchability plateau. Fig. 1 shows a time series of images before and after applying a constant velocity.

3. Single relaxation FENE-P model

Direct measure of the chain stretch is only possible in specialized experiments, such as in the case of labeled DNA [24]. Therefore, we use a finite extensibility nonlinear elastic (FENE) model, presented by Entov and Hinch [19], to estimate the chain configuration and polymer stress as a function of strain using experimental data. This model

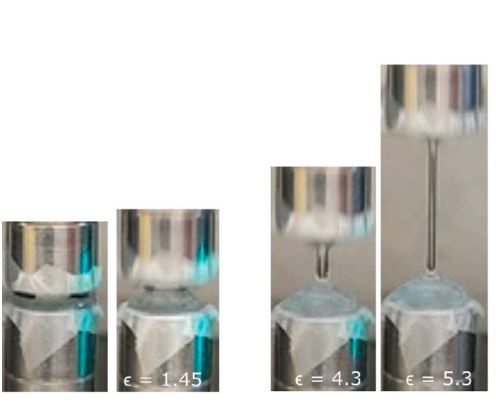






Fig. 1. Capillary necking and filament stretching of a dilute polymer solution on the VADER.

has also been used by others to better understand filament thinning experiments [15,25]. We briefly detail the equations solved to estimate the chain stretch, A_{zz} , and the polymer stress, σ_p . Consider a uniform cylindrical liquid bridge whose radius, R(t), is decreasing as a function of time. Let the axial strain-rate of the axisymmetric extensional flow be $\dot{\epsilon}(t)$, such that the radius decreases via:

$$\frac{\partial R}{\partial t} = -\frac{1}{2}\dot{\epsilon}R(t) \tag{1}$$

from the definition of the Hencky strain, $\epsilon = -2\ln(D(t)/D_0)$, and the Hencky strain rate, $\dot{\epsilon} = \partial \epsilon/\partial t$. The elastic deformation of the polymer coil is described by the normalized conformation tensor, **A**, i.e. a fully relaxed chain has $A_{zz} = A_{rr} = 1$ and the fully stretched chain is given by $A_{zz} = L^2$. Taking into account the microstructural evolution equation:

$$\overset{\nabla}{\mathbf{A}} = \frac{D\mathbf{A}}{Dt} - \mathbf{A}\nabla\mathbf{v} - (\nabla\mathbf{v})^T \mathbf{A} = -\frac{1}{\lambda G} \boldsymbol{\sigma}_{\mathbf{p}}$$
 (2)

where $\overset{\mathbf{v}}{\mathbf{A}}$ denotes the upper-convected derivative, λ denotes the relaxation time of the polymer chain, and $\sigma_{\mathbf{p}}$ is the polymeric stress given by

$$\sigma_{\mathbf{p}} = G\epsilon_{chain} = G(Z\mathbf{A} - \mathbf{I})$$
 (3)

where G is the shear modulus, the parameter Z denotes the correction term accounting for the nonlinearity and the finite extensibility of the chain of fully stretched length L, given by,

$$Z = \frac{L^2}{L^2 + 3 - A_{zz} - 2A_{rr}} \tag{4}$$

where $tr(\mathbf{A})$ denotes the trace of the conformation tensor. From the radial symmetry and uniaxial flow kinematics the evolution equations reduce to two differential equations for A_{zz} and A_{rr} respectively:

$$\frac{dA_{zz}}{dt} = 2\dot{e}A_{zz} - \frac{Z}{\lambda}(A_{zz} - 1) \tag{5}$$

$$\frac{dt}{dA_{rr}} = -\dot{\epsilon}A_{rr} - \frac{Z}{\lambda}(A_{rr} - 1) \tag{6}$$

These equations can be solved subject to the initial conditions of the chains in their fully relaxed state.

$$A_{zz}(0) = A_{rr}(0) = 1 (7)$$

The only parameters that need to be specified are L, λ , and $\dot{\epsilon}$. For 4×10^6 kg/mol PEO, L=227 determined using Ref. [15,26] λ is determined experimentally as detailed below. We depart from the typical solution method, which is to estimate the strain-rate from a thin filament model [25], and instead use experimental data of D(t) to determine

Table 2 Parameters used in the calculation of L.

Parameter	Description	Value	Source
Θ_B	Average bond angle	1.909	[26]
j	Number of bonds of a monomer	3	[26]
Mw_0	[kg/mol] of monomer	0.044	[28,29]
C_{∞}	Ratio for a given monomer	44.1	[26]
ν	Excluded volume coefficient	0.544	[27]
μ	[Pa s] viscosity of solvent	0.001	[26]
ρ	[kg/m ³] density	998	
γ	[N/m] surface tension	0.062	[30]
R_0	[m] radius of plates	0.004	
Mw	[kg/mol] of polymer chain	4×10^{3}	

the local experimental strain-rate, \dot{e} as a function of time as an input into the equations. The experimental \dot{e} values are smoothed using a Whitaker smoothing routine and the values are used directly in the calculation of chain stretch and polymer stress. The equations are solved using MatlabTM ODE15s and the script file is available upon request. The estimated maximum coil length of the polymer, the finite extensibility parameter, is determined by the molecular weight and the excluded volume coefficient characterizing the quality of the solvent [25,27] (see Table 2).

4. Results

There are typically three sequential Regimes of filament stretching for a dilute polymer solution: (1) visco-capillary, (2) Rayleigh instability Regime, and (3) elasto-capillary. Regimes (1) and (3) are defined by the magnitude of the individual force components, i.e. capillary force, viscous force, and elastic force. For example, the visco-capillary thinning Regime is a competition of shear viscosity and capillary forces, while Regime (3) is a competition between capillary and polymer elastic forces. The instability Regime, referred to by Entov and Hinch [19] as the middle-elastic time, is defined by an instability caused by capillary forces and is commonly referred to as the Rayleigh-Plateau instability. This instability occurs at a critical aspect ratio depending on the volume of the filament [31]. Note that a Newtonian fluid, with no elastic effects, is only capable of Regime (1) and (2) [32]. Polymer solutions stretched fast enough to mount sufficient stored elastic energy during Regime (1) can skip Regime (2) and immediately observe Regime (3), as in the experiments of Liang and Mackley [33]. In the case of low-viscosity dilute solutions, it is rare that Regime (2) is avoided, and Regime (3) is achieved by very fast stretching during

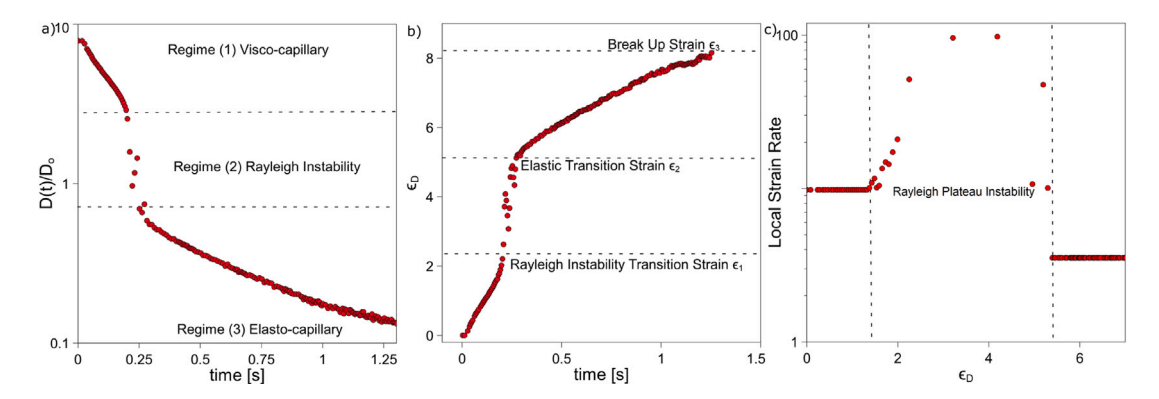


Fig. 2. (a) 960 wppm 20 mm s⁻¹ normalized diameter decay vs. time, (b) 960 wppm 20 mm s⁻¹ ϵ_D vs. time, (c) 960 wppm 7 mm s⁻¹ local strain rate vs. strain.

Regime (2) such that the elastic stress balances the capillary stress [7,34,35]. Regime (3) is typically analyzed to determine a polymer relaxation time from the thinning filament [2,22,27,36]. The three Regimes are typically visualized by monitoring the normalized minimum diameter of a liquid filament as a function of time. Fig. 2(a) shows the initial Newtonian visco-capillary necking Regime, followed by the Rayleigh-Plateau instability transition, and finally by the elastic stretching Regime and final break-up [37,38]. Note that each Regime has a different decay of diameter with time. We hypothesize that the degree to which the steady elastic Regime is observed strongly depends on the state of the chain upon entering Regime (2), i.e. the stretch of the polymer chain in Regime (1) dictates the thinning behavior in the elasto-capillary regime. Thus, this work determines the minimum strain-rate in Regime (1) required to observe steady elastic stretching in Regime (3), and shows that this critical rate is related to the relaxation time of the polymer chain.

For the purpose of this paper, we are interested in the magnitude of the radial Hencky strain, ϵ_D as a function of time. Fig. 2(b) shows Hencky strain versus time for the data in Fig. 2(a). Furthermore, the rate of change of radial Hencky Strain, known as the Hencky strain rate, ϵ_D , is proportional to the inverse of the relaxation time [10,39–41]. Fig. 2(c) shows the local Hencky strain rate as a function of time, which will be later used to calculate other derivative parameters, such as coil stretch and relaxation time. Note that the elasto-capillary Hencky strain rate in Fig. 2(c) is only reported to a Hencky strain of approximately 7, since above this strain the strain rate is no longer constant and begins decreasing. One reason for the decrease in rate is an error in diameter as the resolution of the instrument is approached (i.e. 100 μ m).

The three stretching Regimes are clearly marked in Fig. 2. For this material and experimental conditions, Fig. 2(b) shows that each Regime occurs over approximately two units of strain; however, the rates in these Regimes are very different. It is useful to define three characteristic strains: ϵ_1 , the Rayleigh instability transition strain, ϵ_2 , the elastic transition strain, and ϵ_3 , the maximum measured strain. Note that ϵ_3 is a measure of the instrument limitation in accurately measuring the diameter of the filament ($\epsilon_3 \approx 8$ for the VADER). The rates of deformation observed in Fig. 2(c) show a very interesting result regarding the constant velocity scheme: namely that the constant velocity scheme results in a constant rate of extension in Regime (1). Regime (2) shows an unstable stretching rate that grows to a maximum [42], and then decreases to a steady state value in Regime (3). The steady state value of strain-rate observed in Regime (3) is what previous studies typically use to calculate the relaxation time of the material [43]. We will demonstrate that the strain rate in Regime (1) must be equal to or larger that the rate observed in Regime (3) to accurately measure the longest relaxation time.

Fig. 3 shows Hencky strain as a function of time for a range of velocities (5–100 mm/s) and three concentrations measured in this study; the remainder of the tested concentrations are included in full in the supplementary. For all concentrations, we observe that Regime (1)

is shortening in time for increasing velocity. Thus, the rate of deformation in Regime (1) is increasing with increasing velocity. This is more explicitly shown in Fig. 5. Furthermore, we observe ϵ_1 is independent of the velocity and the concentration and that ϵ_2 is decreasing with increasing velocity for a given concentration. Lastly, we observe that the rate of extension in Regime (2) and Regime (3) are a function of velocity and polymer concentration.

Fig. 4 shows Hencky strain versus time for seven measured concentrations stretched at the same velocity. This figure helps to discern which features of Fig. 3 are rate and concentration dependent. For example, we observe that all seven concentrations have the same initial extension rate in Regime (1), indicating that the initial rate is simply a function of the applied velocity. Conversely, we observe that the transition strain from Regime (2) to Regime (3), i.e. ϵ_2 , is a function of polymer concentration for the same applied initial rate. Lastly, the extension rate observed in Regime (3) is a strong function of polymer concentration, indicating that this rate is a material parameter. As one might expect, the lowest and highest concentration have the highest and lowest strain-rate in Regime (3), respectively, which tracks with the inverse of their expected relaxation times. These important observations are discussed in detail below, with an emphasis on the measurement of relaxation time.

5. Discussion

One surprising result from Fig. 3 is that the constant velocity measurement results in a constant rate experiment in Regime (1). This is better seen in Fig. 5(a) where the average strain-rate of Regime (1) is plotted as a function of applied velocity. Recall that, as shown in Fig. 4, the strain-rate in Regime (1) is not a function of polymer concentration, but is a property of the sample aspect ratio and solution viscosity, which does not vary with concentration for dilute solutions. Note that increasing sample aspect ratio leads to a lower initial extension rate for the same velocity, and vice versa. Different plate sizes, and therefore aspect ratios, would result in a different linear relationship with velocity, and different minimum velocities. Fig. 5(a) shows a linear dependence of the initial strain rate on the plate separation velocity, with a slope of approximately 0.5. The confidence interval of the population varies narrowly with a standard error that increases linearly with velocity, up to a value of 1.4 at 100 mm/s. The fact that the constant velocity experiment leads to a constant rate is advantageous since polymer physics is formulated in terms of normalized timescales, such as the Weissenberg number [44], that involve the rate of extension compared to the polymer relaxation time. Thus the discussion of experimental data will be done in terms of initial extension rate not velocity.

Another observed trend that is important to highlight is the effect of initial strain rate and concentration on the elastic transition strain, ϵ_2 , described in Figs. 2 and 3. Fig. 5(b) shows ϵ_2 as a function of initial strain rate for C=240 wppm. We clearly observe a decreasing function of ϵ_2 for increasing initial strain-rate below 12/s. After which, we

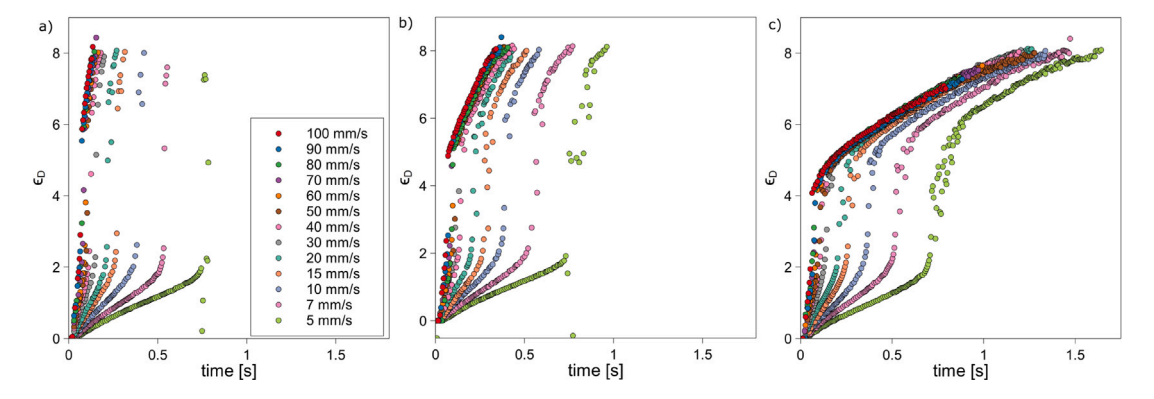


Fig. 3. Hencky strain vs. time for different velocities for three concentrations (a) 30 wppm, (b) 240 wppm, and (c) 960 wppm.

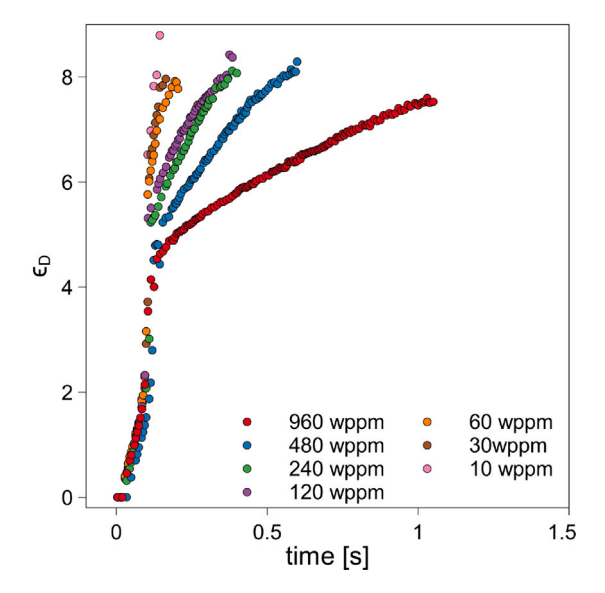


Fig. 4. Various concentrations of polymer in solution measured at 50 mm/s.

observe a plateau in ϵ_2 , demonstrating a rate independent phenomenon. One might propose that this transition in ϵ_2 is related to a transition of stretching the chains at a rate below the inverse relaxation time to stretching faster than the inverse relaxation time. The strain-rate where ϵ_2 becomes rate-independent is a direct measure of the inverse of the polymer relaxation time. It is at this initial strain-rate that we would expect the polymer stress to exceed the capillary stress, allowing for a direct observation of the polymer relaxation time in the third regime. Moreover, the fact that ϵ_2 is rate-independent above a minimum initial strain-rate suggests affine deformation of the polymer molecules above this critical rate.

Fig. 5(c) shows the asymptotic ϵ_2 as a function of concentration, also tabulated in Table 3. As the concentration increases the asymptotic ϵ_2 decreases. This suggests that there is a critical stress for a given initial sample aspect ratio required to achieve longest chain stress relaxation. Current polymer physics scaling laws establish that relaxation time and polymer stress increase with increasing polymer concentration. More specifically, polymer stress, σ_p depends directly on the solution viscosity (for dilute solutions) and shear modulus, G, (for concentrated solutions) which are explicit functions of polymer concentration [19]. This implies that a higher concentration requires less strain (i.e. chain stretch) to achieve a given σ_p , which is the trend observed in Fig. 5(c). Lower concentration solutions require significantly higher strains than concentrated solutions to observe stress relaxation. Thus, an instrument's accessible strain window will limit the measurable concentration for a given polymer.

The practical importance of the elastic transition strain and its relation to the relaxation time are made evident in Fig. 5(d). We observe that the strain-rate measured in Regime (3) is initially a decreasing function of the initial strain rate, until it reaches an asymptotic value. The solid line in Fig. 5(d) is the y = x line, which crosses the experimental data at the asymptotic strain rate. This phenomena occurs in each concentration tested and reveals a fundamental kinematic requirement of measurement: the initial rate must be equal to or faster than 2/3 the inverse relaxation time of the polymer solution in order to observe the correct timescale. The initial extension rate must be large enough that the initial Weissenberg number, Wi = $\lambda \dot{\epsilon} > 2/3$, such that the chains are undergoing stretching in the visco-capillary regime. When this criteria is met, the chains are presumably sufficiently stretched in Regimes (1) and (2), i.e. σ_p is large enough at small strains, to ensure that the longest relaxation mode dominates the dynamics in regime (3), see Table 3 Most importantly, an observed extension rate in regime (3) does not necessarily correspond to the materials relaxation time, and any attempt to extract a relaxation time below Wi < 2/3 will lead to erroneously smaller relaxation times. This is true for all concentrations measured. Note that the requirement of Wi> 2/3 comes from using the analysis of Entov and Hinch to determine the longest relaxation time.

Table 3 shows all the measured and derived values for the seven concentrations studied. As noted in the table, the lowest initial strain-rate (denoted as initial \dot{e}) where an asymptotic thinning rate is observed and is either larger or approximately equal to the measured Elastic \dot{e} . Above this initial rate, the Elastic \dot{e} is independent of the initial \dot{e} . The asymptotic relaxation time for each concentration was calculated using the definition in Table 1. One exception is 10 wppm, whereby no asymptotic elastic \dot{e} was observed for the achievable rates using the VADER. This brings up the important point that not all relaxation times are accessible by a machine with a limited initial plate separation velocity range. For example, using the relationship between initial \dot{e} and plate velocity in Fig. 5 for the sample aspect ratio used in this study, a predicted minimum plate separation velocity, V_{min} required to measure a relaxation time, λ , is given by

$$V_{min} = \frac{890 \text{ [mm]}}{\lambda \text{ [ms]}} \tag{8}$$

This equation allows the limit of a given experimental setup to be determined simply by knowing its maximum velocity.

However, initial plate separation velocity is not the only limitation to accurately measuring material relaxation times. Another important limit is the issue of limited data collection speeds. For example, although the VADER can achieve velocities up to 600 mm/s, which would theoretically allow for the accurate measurement of $\lambda=1.45$ ms, it is limited by a data collection rate of 50 points per second, which limits the VADER to an elasto-capillary thinning rate of approximately 40 1/s.

The asymptotic relaxation times in Table 3 are compared with previously published results in Fig. 6 for the same molecular weight PEO. Note that the data for this work and that of Deblais et al. use identical

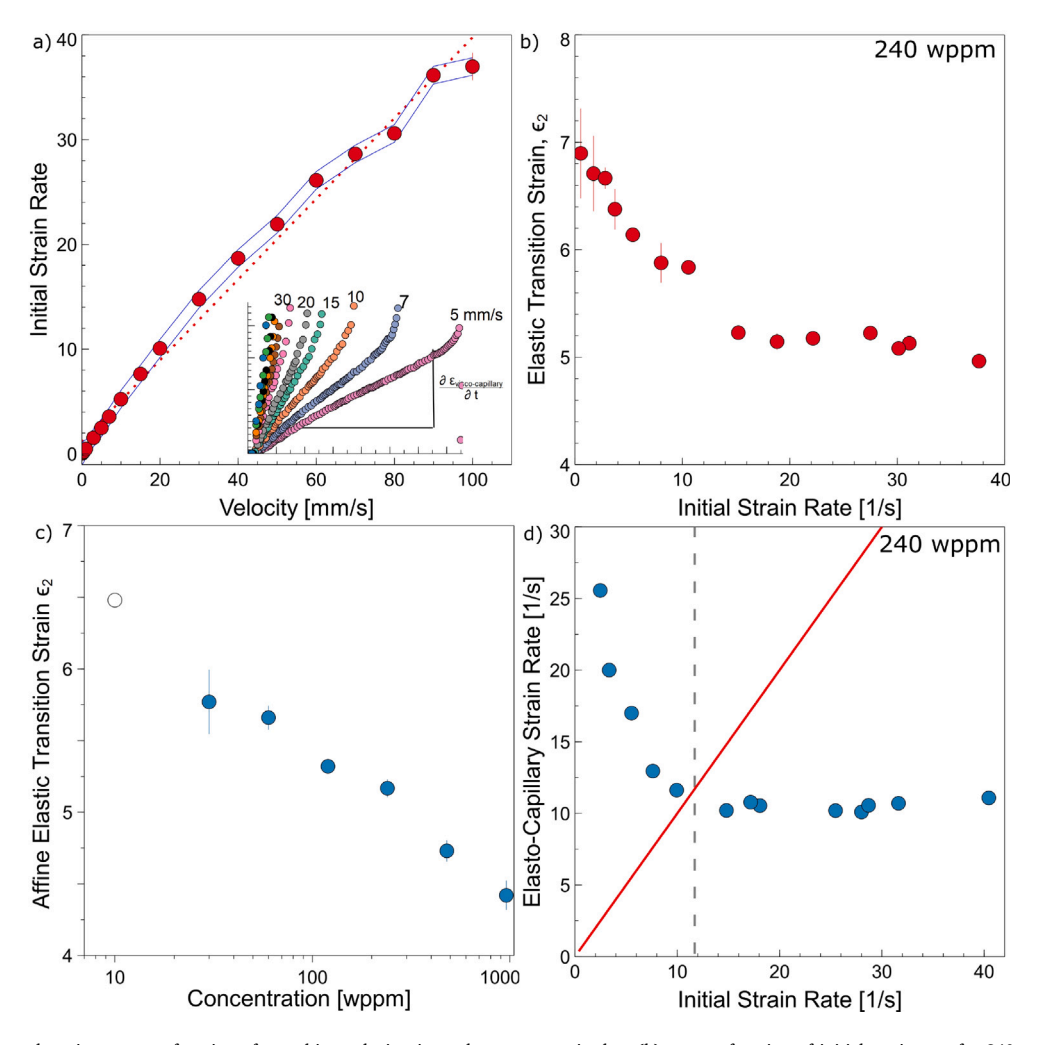


Fig. 5. (a) initial measured strain rate as a function of stretching velocity, inset shows raw strain data (b) ϵ_2 as a function of initial strain rate for 240 wppm, (c) asymptotic ϵ_2 as a function of concentration, and (d) elasto-capillary thinning rate as a function of initial strain rate for 240 wppm.

 $\begin{tabular}{ll} \textbf{Table 3} \\ \textbf{Asymptotic values of derived variables from constant velocity stretching of different PEO concentrations. Note that the Elastic \hat{e} represents an average value. } \end{tabular}$

C [wppm]	C/Ca	Initial $\dot{\epsilon}$	Elastic $\dot{\epsilon}$ [1/s]	Relaxation time [ms]	ϵ_2
10	0.013	40 ^a	67.1	9.94 ^a	6.48 ^a
30	0.039	43.8	33.5	19.92	5.77
60	0.078	24.3	21.6	30.88	5.66
120	0.156	11	11.0	60.64	5.32
240	0.312	11.7	10.5	63.36	5.167
480	0.623	8.1	7.31	91.26	4.73
960	1.247	3.35	3.36	198.64	4.42

^a Indicates the minimum measured derived variable not the asymptotic value, as no asymptote was achieved.

material sourcing and target concentrations for direct comparisons. Although the trends in λ with concentration are similar between the two studies, the values measured using DOS are consistently lower. One explanation for the difference in measured relaxation time is that the DOS method did not achieve the required initial extension rate to measure the longest relaxation time. Unfortunately, the stretching of the DOS filament at early times is not reported and therefore this argument could not be validated. Other explanations for this discrepancy could include polymer polydispersity, incidental Mw degradation from sample preparation and storage, and slight variability in concentrations due to evaporation. All other reported relaxation times in Fig. 6 are lower than the asymptotic relaxation times measured in this study. This is again in support of our arguments that sufficiently fast initial

stretching leads to a measure of the longest relaxation time. However, this could not be quantitatively confirmed since the startup flows were not reported in the studies. Thus, it is possible that the differences are due to material differences [22]. Note that all relaxation times reported in this study are above the estimated Zimm time, calculated using $\lambda_{zimm} = (F[\eta]Mw\eta_0)/(N_Ak_BT) = 0.001$ s, where F = 0.463 [45], $[\eta] = 1.408$ m³/kg [46], Mw = 4000 kg/mol, $\eta_0 = 0.00095$ Pa s, N_A is Avogadro's number, k_B is the Boltzmann constant, and T is the temperature in Kelvin. Concentrations dilute enough to approach the Zimm relaxation time also approach such low stress of even a fully uncoiled chain that the polymer may carry less stress than the solvent [271].

The results and discussion above suggest that the state of the polymer chain just before entering the instability is a key parameter to measuring stress relaxation in the final thinning regime. To test this idea, we used a single relaxation FENE model to estimate the chain stretch as a function of strain during different stretching velocities. The experimental $D_{min}(t)$ was used to determine $\dot{e}(t)$ and used as an input into the model to calculate A_{zz} and σ_p as a function time and filament strain, see Model section for details. A subset of the experimental data used for the calculation are in Fig. 7, with additional data sets showing the viscous force included in the supplementary. Fig. 7 shows A_{zz} as a function of filament strain for five stretching velocities. Recall that for 240 wppm, the minimum velocity needed to achieve a high enough initial strain rate to observe rate-independent stress relaxation was 20 mm/s, and all lower velocities lead to erroneous relaxation times. A comparison of A_{zz} as a function of ϵ_D shows that

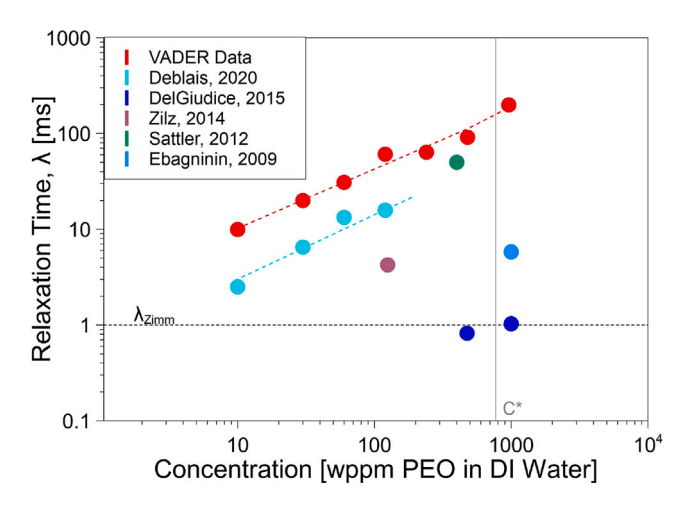


Fig. 6. Comparison of relaxation time measured in this study compared to relaxation times reported in the literature for the same molecular weight PEO [14,42,47-49].

the 5 mm/s experiment does not introduce significant chain stretch during the visco-capillary stretching regime (i.e. $\epsilon_D <$ 1.8). Thus most of the stretching occurs in the Rayleigh–Plateau instability regime, and maximum stretch is only reached at very large ϵ_D . At 20 mm/s, we observe considerably more stretching during the visco-capillary stretching regime, and a much shorter strain required to reach maximum stretch. At velocities above 20 mm/s, the chain stretch is almost a linear function of ϵ_D until it reaches the chain's maximum extensibility.

The effect of velocity on the chain stretch is more pronounced in Fig. 7(b), which shows the polymer stress as a function of filament strain. At 5 mm/s, below the minimum initial $\dot{\epsilon}$, we observe that the polymer stress is always below the capillary stress until very high strains near the limitation of measurement (100 µm diameters), where σ_n exceeds the capillary stress. At 20 mm/s, i.e., the minimum velocity to observe stress relaxation, we observe that the polymer stress exceeds the capillary stress at $\epsilon_D \approx 5.2$, followed by a brief but observable stress relaxation of the chain. At velocities above 20 mm/s, we see the polymer stress exceeds the capillary stress at smaller ϵ_D followed by a very long stress relaxation period. These results clearly suggest that the initial stretching of the chain in the visco-capillary stretching regime leads to the polymer stress exceeding the capillary stress at small ϵ_D , and stress relaxation occurs. The higher the velocity, the smaller the ϵ_D where σ_p exceeds the capillary stress and the larger the stress relaxation window. This point is quite surprising, since Entov and Hinch suggest that in Regime (3) the elastic stress exactly balances the capillary stress [19]. The fact that the model does not give rise to this fact, either means that the model or model parameters are wrong and are not appropriate to describe the stress state of the chain, or that the experiment performed above is leading to a different mechanism for elasto-capillary thinning.

A more subtle point regarding the simulation results in Fig. 7(a-b) is that there is a minimum chain stretch required when exiting the visco-capillary stretching regime, i.e. stretching regime (1), to induce stress relaxation. The maximum induced strain in stretching regime (1) for a low-viscosity fluid is determined by its initial aspect ratio and volume [31]. For the measurements in this study, the maximum strain is $\epsilon_D=1.8$. An analysis of the A_{zz} at $\epsilon_D=1.8$ gives a minimum chain stretch needed in regime (1) to achieve stress relaxation. Fig. 8(a) demonstrates there is more chain stretch with increasing initial strain rate (i.e. velocity) until at high enough rates the chain stretch reaches an asymptotic value, $A_{zz}=11.5$. This suggests that at high enough rates, the chains are undergoing affine deformation. Interestingly, this analysis was repeated for all concentrations and the asymptotic A_{zz} in regime (1) is not a strong function of concentration. Combining these results, we observe that there is a minimum chain stretch that

must be achieved in regime (1) to observe stress relaxation, and this only occurs when the rate of deformation in regime (1) is greater than 2/3 the inverse relaxation time. Furthermore, higher polymer concentrations, longer relaxation times, reach a polymer stress greater than the capillary stress at earlier strains and therefore have a larger strain window in regime (3).

6. Additional advantages of the constant velocity scheme

One major issue in standard CaBER measurements is the inertial recoil induced upon sudden stoppage of the top plate. The recoil makes it difficult to capture the minimum thinning radius [14]. One suggested solution to avoid recoil is the slow retraction method (SRM) [20]. However, this method is clearly at odds with the results presented here, and most likely explains the very low relaxation times measured using this method for 500 wppm PEO (Mw = 1×10^6 g/mol) in water of $\lambda=1.38$ ms. This is supported by relaxation time, $\lambda=2.4$ ms, measured using the free jet extensional rheometer measurement of the same concentration and molecular weight in water and glycol [50]. Instead, our results here show that a constant plate separation velocity limits recoil and ensures that the initial rate is large enough to ensure that the thinning in regime (3) is rate-independent. In fact, multiple velocities should be applied to determine whether a consistent relaxation time is observed.

7. Stretchability index

It is clear from users of capillary breakup indexers that the relaxation time, although a useful quantity, does not capture all the important physics of stretching. For this reason, many users of capillary breakup measurements rely on shape and image analysis during the stretching process to compare different materials. Such analysis is time consuming and not necessarily systematic. In this work, we propose a different measure of the thinning behavior using the kinematic relationship between the radial Hencky strain, ϵ_D , and the axial Hencky strain, ϵ_z , measured during stretching. The relationship between ϵ_D and ϵ_z is a function of the sample aspect ratio, the separation velocity, and the balance of stresses in the liquid bridge. Fig. 9(a) shows ϵ_z as a function of ϵ_D for a wide range of stretching velocities. Note that due to the constant velocity imposed the y-axis is essentially the log of time, which means it is qualitatively similar to the inverse of Fig. 3c. However, the figures are quantitatively different since ϵ_Z is time scaled by velocity/ L_a and represents the dimensionless axial strain. This is significant in that both minimum kinematic strain parameters and maximum material elasticity can be identified. At low ϵ_D , i.e. the visco-capillary regime $\epsilon_D < 1.8$, there is almost no dependence of the kinematics on the stretching rate. For 1.8 < ϵ_D < 5, we observe for all velocities a significant change in ϵ_D with almost no change in ϵ_z . This region denotes the instability stretching regime, whereby the filament thins on its own. Finally, for $\epsilon_D > 5$, we observe a strong dependence of ϵ_z with stretching rate, which denotes the elastocapillary stretching regime. The kinematic relationship in this regime is an important indicator for how much a liquid bridge of this material can be stretched at a given velocity before the bridge breaks.

One measure of the materials stretchability is the slope of the kinematic curve in regime (3), see inset Fig. 9(a). Note that the stretchability factor is analogous to the inverse Poisson ratio used in solid mechanics. There are two important stretchability limits that have been determined experimentally and theoretically, namely viscous stretching, which has a slope of 2/3 and elastic stretching, which has a slope of 1 [51,52]. Note that surface tension is omitted in the original definition of these limits. Fig. 9(b) shows the stretchability as a function of separation velocity for 30 and 480 wppm PEO solutions, with the data for other concentrations included in the supplementary. For both concentrations, the stretchability of the material increases with increasing velocity and approach an asymptotic value. The asymptotic

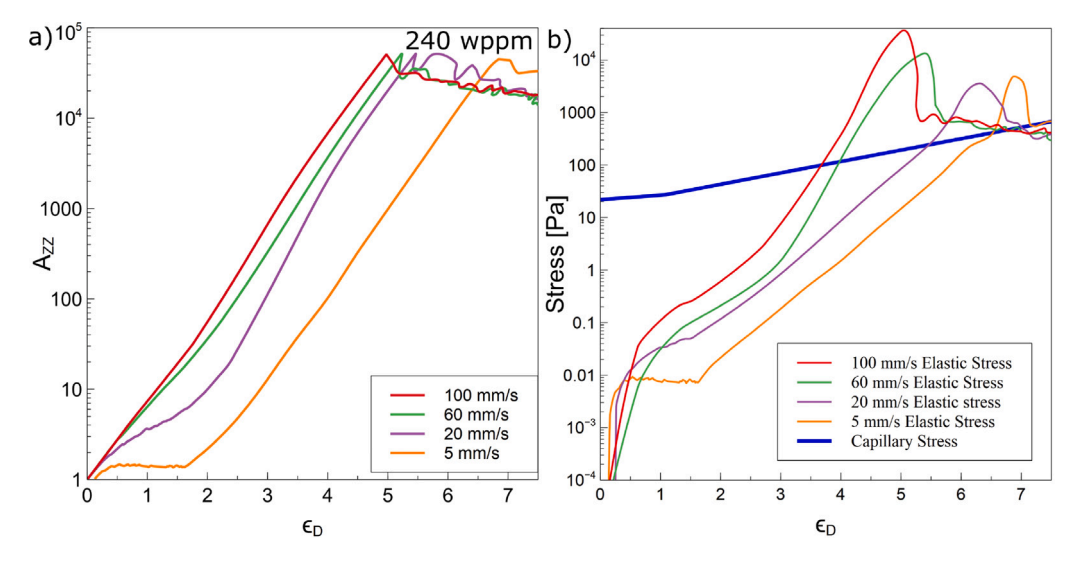


Fig. 7. 240 wppm, velocities 5 mm/s (initial $\dot{\epsilon}=2.5~s^{-1}$), 20 mm/s (initial $\dot{\epsilon}=10~s^{-1}$), 60 mm/s (initial $\dot{\epsilon}=2.5~s^{-1}$), 100 mm/s (initial $\dot{\epsilon}=37~s^{-1}$) (a) Calculated Azz as a function of filament strain ϵ_D using experimental local strain-rate data (b) polymer and capillary stress as a function of filament strain, ϵ_D using experimental local strain-rate data. For all velocities, regime (1) to regime (2) transition occurs at a strain of approximately 1.8, but for the transition to regime (3) this occurs at 4.98 for 100 mm/s, 5.22 for 60 mm/s, 5.77 for 20 mm/s, and 6.85 for 5 mm/s.

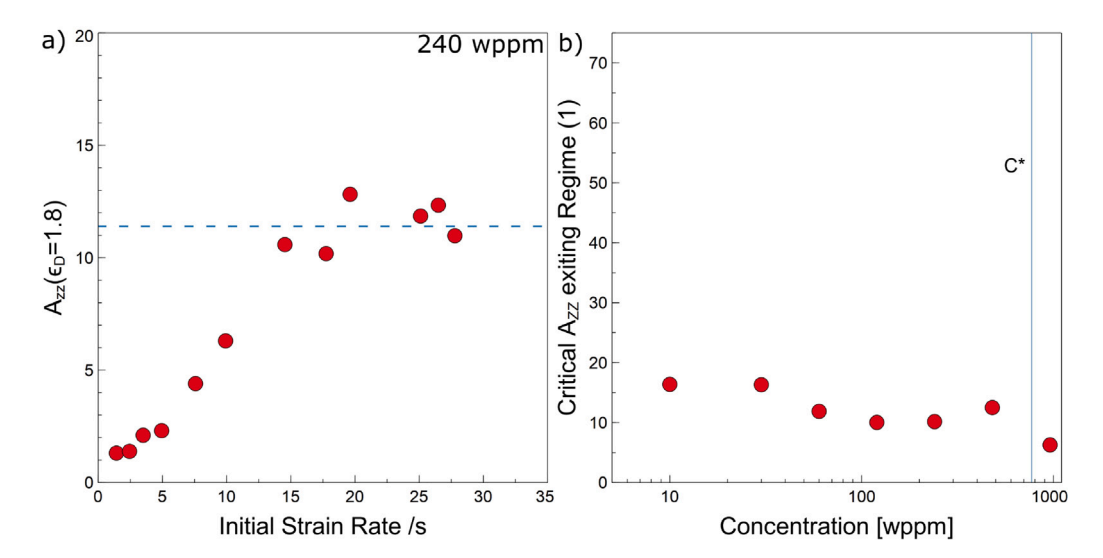


Fig. 8. (a) A_{zz} determined at ϵ_D , the maximum strain in regime (1) versus the initial extension rate, (b) the asymptotic A_{zz} as a function of polymer concentration.

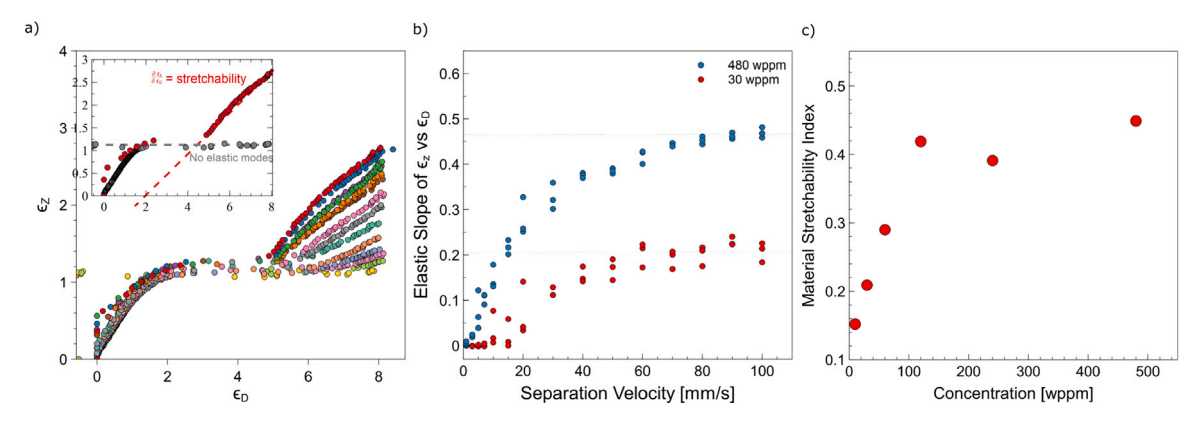


Fig. 9. (a) shows ϵ_z vs. ϵ_D for 960 wppm at all velocities measured, the inset shows the definition of the stretchability factor determined from $d\epsilon_z/d\epsilon_D$ in the elastic stretching regime (b) stretchability factor as a function of plate separation velocity for 30 and 480 wppm, and (c) the asymptotic stretchability factor, referred to as the material stretchability index, as a function of concentration.

value is a material parameter that is proportional to the polymeric stress induced in the material during the visco-capillary and instability stretching regimes. Fig. 9(c) shows the asymptotic stretchability, which we denote as the stretchability index, for all PEO concentrations tested, except 960 wppm. Unlike the dilute concentrations, 960 wppm does not approach an asymptotic stretchability factor. Recall that C* for PEO solutions is 770 wppm [23]. Extrapolation of the results shows that 960 wppm could exhibit fully elastic behavior (a slope of 1), at an estimated velocity of 139 mm/s. This suggests that concentrations below the C^* are distinct from the semi-dilute region, and not capable of fully elastic behavior. For the dilute concentrations, the asymptotic stretchability factor increases significantly at low concentrations, but reaches a plateau of approximately 0.4 at 120 wppm. Overall, the stretchability factor and index are unique material parameters, which define the degree of stretching for a given velocity and the overall shape of the material during stretching. We expect that these properties, in addition to the material relaxation time, will be very useful parameters in making correlations to process parameters.

8. Conclusion

This work highlights the importance of chain stretch in the viscocapillary stretching regime to achieve a rate-independent relaxation time in a capillary breakup measurement. We showed that the stretching rate in the visco-capillary regime must be larger than 2/3 the inverse relaxation time. Otherwise, below the minimum initial stretching rate, the relaxation time measured in the elasto-capillary regime is rate dependent, smaller than the longest polymer relaxation time, and not a material parameter. Comparison with literature revealed that many experimental studies reported much lower relaxation times for the same molecular weight polymer concentrations studied here. We speculate that these studies did not reach the minimum visco-capillary stretching rate. Furthermore, these results may explain the discrepancy in measured relaxation times using different capillary breakup measuring techniques [15]. It is likely in comparing slow retraction CaBER with naturally very high rate ROJER, that the initial stretching rate in ROJER is significantly faster than that in the CaBER testing. Different scaling factors may not be necessary across methods when minimum chain stretch requirements are met. Unfortunately, since these studies did not report the initial stretching kinematics, we can only speculate.

Another interesting result is that the strain required to achieve regime (3), ϵ_2 , is a strong function of the initial stretching rate and concentration, and was shown to correlate to the material relaxation time. There is a minimum strain required on the filament to ensure that the correct relaxation time of the polymer is observed in the elasto-capillary thinning regime. Lower polymer concentrations required a higher filament strain to observe a rate-independent relaxation time. These results can be explained by understanding the relationship between filament strain and molecular strain. At high enough initial stretching rates, the polymer chain should undergo affine deformation, and the polymer stress should increase with filament strain. A higher filament strain required for lower concentrations indicates that there is a minimum chain stretch for a given concentration to measure the longest relaxation time. These results have important implications for experiments. For example, the capillary stress depends on the curvature of the filament, i.e. the diameter, and thus larger diameter filaments could be used to lower the required filament strain to observe rate-independent stress relaxation. Furthermore, the fastest initial strain-rate imposed and the data acquisition time of the instrument determines the fastest rateindependent relaxation time that can be measured. For the VADER, the data acquisition time sets the measurable relaxation time to above 26 ms.

Coupling the experimental results with a single relaxation FENE-P model, we showed that there is indeed a minimum chain stretch required in the visco-capillary regime to observe a rate-independent

relaxation time in regime (3), which depends on the polymer concentration. The model suggests that active stretching in regime (1) leads to the polymer stress exceeding the capillary stress, followed by stress relaxation. Note that this mechanism is fundamentally different than that proposed by Entov and Hinch, whereby regime (3) was characterized by a balance of elastic and capillary stresses. These results either suggest that the model or model parameters are not appropriate to characterize the polymer stress, or active stretching regime (1) leads to a different type of experimental approach to measuring the longest relaxation time.

In many cases, the measure of relaxation time is not sufficient to correlate material properties to observed phenomena, and thus additional indexes are sought for material characterization. One standard practice in capillary breakup experiments is to use a camera to observe the shape of the filament during breakup, and compare the filament shape as a function of time. In this work, we show that a variable stretching rate, coupled with a direct measure of axial and radial filament strain allows for a kinematic description of the material, which is denoted as the stretchability factor. More specifically, the stretchability factor is the slope of the kinematic curve in regime (3), and is a direct measure of the materials stretchability. The stretchability factor for a given sample geometry is a function of plate separation velocity and approaches an asymptotic value at high enough stretching rates, i.e. faster than 2/3 the inverse relaxation time. The asymptotic value is denoted as the Material's Stretchability Index and is shown to be a function of polymer concentration. At larger concentrations, below C^* , the Material Stretchability Index reaches an asymptotic value. The stretchability index should prove a useful index in comparing materials for capillary breakup applications.

CRediT authorship contribution statement

Ann Aisling: Writing – original draft, Methodology, Investigation, Formal analysis, Data curation, Conceptualization. Renee Saraka: Writing – review & editing, Methodology, Investigation, Data curation. Nicolas J. Alvarez: Writing – review & editing, Supervision, Project administration, Methodology, Funding acquisition, Formal analysis, Conceptualization.

Declaration of competing interest

The authors declare the following financial interests/personal relationships which may be considered as potential competing interests: Nicolas J. Alvarez reports financial support was provided by National science Foundation Division of Chemical Bioengineering Environmental and Transport Systems. Nicolas J. Alvarez reports a relationship with Rheo Filament ApS that includes: board membership. Nicolas J. Alvarez has patent issued to Rheo Filament ApS. If there are other authors, they declare that they have no known competing financial interests or personal relationships that could have appeared to influence the work reported in this paper.

Data availability

Data will be made available on request.

Acknowledgments

This work was supported by the National Science Foundation, United States under grant no. CBET-1847140. AA and NJA would like to thank Gareth McKinley for his suggestions and feedback on the revised manuscript. AA would like to thank Jelena Djuric for help with code used for data analysis and management.

Appendix A. Supplementary data

Supplementary material related to this article can be found online at https://doi.org/10.1016/j.jnnfm.2024.105321.

References

- [1] L. Campo-Deaño, C. Clasen, The slow retraction method (SRM) for the determination of ultra-short relaxation times in capillary breakup extensional rheometry experiments, J. Non-Newton. Fluid Mech. 165 (2010) 1688–1699, http://dx.doi.org/10.1016/j.jnnfm.2010.09.007.
- [2] L.E. Rodd, T.P. Scott, J.J. Cooper-White, G.H. McKinley, Capillary break-up rheometry of low-viscosity elastic fluids, Appl. Rheol. 15 (2005) http://dx.doi. org/10.1515/arh-2005-0001.
- [3] O. Arnolds, H. Buggisch, D. Sachsenheimer, N. Willenbacher, Capillary breakup extensional rheometry (CaBER) on semi-dilute and concentrated polyethyleneoxide (PEO) solutions, Rheol. Acta 49 (2010) http://dx.doi.org/10.1007/s00397-010-0500-7. Peo.
- [4] B. Yesilata, C. Clasen, G.H. McKinley, Nonlinear shear and extensional flow dynamics of wormlike surfactant solutions, J. Non-Newton. Fluid Mech. 133 (2006) http://dx.doi.org/10.1016/j.jnnfm.2005.10.009.
- [5] M.S. Oliveira, R. Yeh, G.H. McKinley, Iterated stretching, extensional rheology and formation of beads-on-a-string structures in polymer solutions, J. Non-Newton. Fluid Mech. 137 (2006) http://dx.doi.org/10.1016/j.jnnfm.2006.01.
- [6] P.C. Sousa, E.J. Vega, R.G. Sousa, J.M. Montanero, M.A. Alves, Measurement of relaxation times in extensional flow of weakly viscoelastic polymer solutions, Rheol. Acta 56 (2017) 11–20, http://dx.doi.org/10.1007/s00397-016-0980-1, PEO in water/glycerol 10⁶ (don't see results for this?) Polyacrylamine in water 18 ×10⁶.
- [7] Y. Amarouchene, D. Bonn, J. Meunier, H. Kellay, Inhibition of the finite-time singularity during droplet fission of a polymeric fluid, Phys. Rev. Lett. 86 (2001) 3558–3561, http://dx.doi.org/10.1103/PhysRevLett.86.3558.
- [8] J.J. Cooper-White, J.E. Fagan, V. Tirtaatmadja, D.R. Lester, D.V. Boger, Drop formation dynamics of constant low-viscosity, elastic fluids, J. Non-Newton. Fluid Mech. 106 (2002) http://dx.doi.org/10.1016/S0377-0257(02)00084-8, Peo but with glycerol.
- [9] J. Dinic, M. Biagioli, V. Sharma, Pinch-off dynamics and extensional relaxation times of intrinsically semi-dilute polymer solutions characterized by drippingonto-substrate rheometry, J. Polym. Sci. B 55 (2017) 1692–1704, http://dx.doi. org/10.1002/polb.24388.
- [10] J. Dinic, V. Sharma, Macromolecular relaxation, strain, and extensibility determine elastocapillary thinning and extensional viscosity of polymer solutions, Proc. Natl. Acad. Sci. USA 116 (2019) http://dx.doi.org/10.1073/pnas. 1820277116.
- [11] K.W. Hsiao, J. Dinic, Y. Ren, V. Sharma, C.M. Schroeder, Passive non-linear microrheology for determining extensional viscosity, Phys. Fluids 29 (2017) http://dx.doi.org/10.1063/1.4993736.
- [12] L.N. Jimenez, J. Dinic, N. Parsi, V. Sharma, Extensional relaxation time, pinch-off dynamics, and printability of semidilute polyelectrolyte solutions, Macromolecules 51 (2018) http://dx.doi.org/10.1021/acs.macromol.8b00148.
- [13] M. Rosello, S. Sur, B. Barbet, J.P. Rothstein, Dripping-onto-substrate capillary breakup extensional rheometry of low-viscosity printing inks, J. Non-Newton. Fluid Mech. 266 (2019) http://dx.doi.org/10.1016/j.jnnfm.2019.03.006.
- [14] A. Deblais, M.A. Herrada, J. Eggers, D. Bonn, Self-similarity in the breakup of very dilute viscoelastic solutions, J. Fluid Mech. (2020) http://dx.doi.org/10. 1017/jfm.2020.765.
- [15] W. Mathues, S. Formenti, C. McIlroy, O.G. Harlen, C. Clasen, Caber vs ROJER— Different time scales for the thinning of a weakly elastic jet, J. Rheol. 62 (2018) 1135–1153, http://dx.doi.org/10.1122/1.5021834.
- [16] V. Sharma, S.J. Haward, J. Serdy, B. Keshavarz, A. Soderlund, P. Threlfall-Holmes, G.H. McKinley, The rheology of aqueous solutions of ethyl hydroxy-ethyl cellulose (EHEC) and its hydrophobically modified analogue (hmEHEC): Extensional flow response in capillary break-up, jetting (ROJER) and in a cross-slot extensional rheometer, Soft Matter 11 (2015) 3251–3270, http://dx.doi.org/10.1039/c4sm01661k.
- [17] B. Keshavarz, V. Sharma, E.C. Houze, M.R. Koerner, J.R. Moore, P.M. Cotts, P. Threlfall-Holmes, G.H. McKinley, Studying the effects of elongational properties on atomization of weakly viscoelastic solutions using Rayleigh ohnesorge jetting extensional rheometry (ROJER), J. Non-Newton. Fluid Mech. 222 (2015) 171–189, http://dx.doi.org/10.1016/j.jnnfm.2014.11.004.
- [18] P.K. Bhattacharjee, A.G. McDonnell, R. Prabhakar, L.Y. Yeo, J. Friend, Extensional flow of low-viscosity fluids in capillary bridges formed by pulsed surface acoustic wave jetting, New J. Phys. 13 (2011) http://dx.doi.org/10.1088/1367-2630/13/2/023005.
- [19] V.M. Entov, E.J. Hinch, Effect of a spectrum of relaxation times on the capillary thinning of a filament of elastic liquid, J. Non-Newton. Fluid Mech. 72 (1997) 31–53.

- [20] L. Campo-Deaño, C. Clasen, The slow retraction method (SRM) for the determination of ultra-short relaxation times in capillary breakup extensional rheometry experiments, J. Non-Newton. Fluid Mech. 165 (2010) http://dx.doi.org/10.1016/j.innfm.2010.09.007.
- [21] A. Gaillard, M. Roché, S. Lerouge, C. Gay, L. Lebon, L. Limat, Viscoelastic liquid curtains: Experimental results on the flow of a falling sheet of polymer solution, J. Fluid Mech. 873 (2019) 358–409, http://dx.doi.org/10.1017/jfm.2019.389.
- [22] S.L. Anna, G.H. McKinley, Elasto-capillary thinning and breakup of model elastic liquids, J. Rheol. 45 (2001) 115–138, http://dx.doi.org/10.1122/1.1332389.
- [23] W.W. Graessley, Polymer chain dimensions and the dependence of viscoelastic properties on concentration, molecular weight and solvent power, 1980.
- [24] C.M. Schroeder, H.P. Babcock, E.S. Shaqfeh, S. Chu, Observation of polymer conformation hysteresis in extensional flow, Science 301 (2003) http://dx.doi. org/10.1126/science.1086070.
- [25] C. Wagner, L. Bourouiba, G.H. McKinley, An analytic solution for capillary thinning and breakup of FENE-P fluids, J. Non-Newton. Fluid Mech. 218 (2015) 53–61, http://dx.doi.org/10.1016/j.jnnfm.2015.01.011.
- [26] J. Brandrup, E.H. Immergut, E.A. Grulk, Polymer Handbook, fourth ed., Wiley, 1999
- [27] C. Clasen, J. Eggers, M.A. Fontelos, J. Li, G.H. McKinley, The beads-on-string structure of viscoelastic threads, J. Fluid Mech. 556 (2006) 283–308, http: //dx.doi.org/10.1017/S0022112006009633.
- [28] B.R. Elbing, Impact of polymer degradation on past studies of the mean velocity profile in turbulent boundary layers, J. Fluids Eng. Trans. ASME 143 (2021) http://dx.doi.org/10.1115/1.4050517.
- [29] M. Grandbois, M. Beyer, M. Rief, H. Clausen-Schaumann, H.E. Gaub, How strong is a covalent bond, Science 283 (1999) http://dx.doi.org/10.1126/science.283. 5408.1727.
- [30] M.W. Kim, Surface activity and property of polyethyleneoxide (PEO) in water, Colloids Surf. A 128 (1997) http://dx.doi.org/10.1016/S0927-7757(96)03918-0.
- [31] J.M. Barakat, Z. Hinton, N.J. Alvarez, T.W. Walker, Surface-tension effects in oscillatory squeeze flow rheometry, Phys. Fluids 33 (2021) http://dx.doi.org/10. 1063/5.0072869.
- [32] J. Eggers, E. Villermaux, Physics of liquid jets, Rep. Progr. Phys. 71 (2008) http://dx.doi.org/10.1088/0034-4885/71/3/036601.
- [33] R.F. Liang, M.R. Mackley, Rheological characterization of the time and strain dependence for polyisobutylene solutions, J. Non-Newton. Fluid Mech. 52 (1994) 387–405.
- [34] M. Goldin, J. Yerushalmi, R. Pfeffer, R. Shinnar, Breakup of a laminar capillary jet of a viscoelastic fluid, J. Fluid Mech. 38 (1969) http://dx.doi.org/10.1017/ S0022112069002540.
- [35] V.M. Entov, A.L. Yarin, Influence of elastic stresses on the capillary breakup of jets of dilute polymer solutions, Fluid Dyn. 19 (1984) http://dx.doi.org/10.1007/ BF01090901.
- [36] A.V. Bazilevskii, V.M. Entov, M.M. Lerner, A.N. Rozhkov, Failure of polymer solution filaments, Polym. Sci. Ser. A 39 (1997).
- [37] Y. Christanti, L.M. Walker, Surface tension driven jet break up of strain-hardening polymer solutions, J. Non-Newton. Fluid Mech. 100 (2001) 9–26.
- [38] D.W. Bousfield, R. Keunings, G. Marrucci, M.M. Denn, Nonlinear analysis of the surface tension driven breakup of yiscoelastic filaments, J. Non-Newton. Fluid Mech. 21 (1986) 79–97.
- [39] G.H. McKinley, A. Tripathi, How to extract the Newtonian viscosity from capillary breakup measurements in a filament rheometer, J. Rheol. 44 (2000) 653–670, http://dx.doi.org/10.1122/1.551105.
- [40] G.H. McKinley, Visco-elasto-capillary thinning and break-up of complex fluids, Rheol. Rev. 3 (2005).
- [41] J.H. Snoeijer, A. Pandey, M.A. Herrada, J. Eggers, The relationship between viscoelasticity and elasticity: Viscoelasticity and elasticity, Proc. R. Soc. Lond. Ser. A Math. Phys. Eng. Sci. 476 (2020) http://dx.doi.org/10.1098/rspa.2020. 0419.
- [42] R. Sattler, S. Gier, J. Eggers, C. Wagner, The final stages of capillary break-up of polymer solutions, Phys. Fluids 24 (2012) http://dx.doi.org/10.1063/1.3684750.
- [43] E. Turkoz, J.M. Lopez-Herrera, J. Eggers, C.B. Arnold, L. Deike, Axisymmetric simulation of viscoelastic filament thinning with the Oldroyd-B model, J. Fluid Mech. 851 (2018) http://dx.doi.org/10.1017/jfm.2018.514.
- [44] R. Poole, The British society of rheology the Deborah and Weissenberg numbers, Rheol. Bull. 53 (2012).
- [45] D.B. L. Rodd, G. McKinley, Role of the elasticity number in the entry flow of dilute polymer solutions in micro-fabricated contraction geometries, J. Non-Newton. Fluid Mech. 170–191 (2007) http://dx.doi.org/10.1016/j.jnnfm.2007. 02.006.
- [46] V. Tirtaatmadja, H.G. McKinley, J.J. Cooper-White, Drop formation and breakup of low viscosity elastic fluids: Effects of molecular weight and concentration, Phys. Fluids 18 (2006) http://dx.doi.org/10.1063/1.2190469.
- [47] F.D. Giudice, G. D'Avino, F. Greco, I.D. Santo, P.A. Netti, P.L. Maffettone, Erratum: Rheometry-on-a-chip: Measuring the relaxation time of a viscoelastic liquid through particle migration in microchannel flows (lab on a chip miniaturisation for chemistry and biology (2015) 15 (783-792)), Lab Chip 16 (2016) 1088, http://dx.doi.org/10.1039/c6lc90028c.

- [48] J. Zilz, C. Schäfer, C. Wagner, R.J. Poole, M.A. Alves, A. Lindner, Serpentine channels: Micro-rheometers for fluid relaxation times, Lab Chip 14 (2014) 351–358, http://dx.doi.org/10.1039/c3lc50809a.
- [49] K.W. Ebagninin, A. Benchabane, K. Bekkour, Rheological characterization of poly(ethylene oxide) solutions of different molecular weights, J. Colloid Interface Sci. 336 (2009) 360–367, http://dx.doi.org/10.1016/j.jcis.2009.03.014.
- [50] Y. Christanti, L.M. Walker, Effect of fluid relaxation time of dilute polymer solutions on jet breakup due to a forced disturbance, J. Rheol. 46 (2002) 733–748, http://dx.doi.org/10.1122/1.1463418.
- [51] G.H.M. Stephen H. Spiegelberg, The role of end-effects on measurements of extensional viscosity in filament stretching rheometers, J. Non-Newton. Fluid Mech. 64 (1996) http://dx.doi.org/10.1016/0377-0257(96)01439-5.
- [52] J.M.R. Marín, J.K. Huusom, N.J. Alvarez, Q. Huang, H.K. Rasmussen, A. Bach, A.L. Skov, O. Hassager, A control scheme for filament stretching rheometers with application to polymer melts, J. Non-Newton. Fluid Mech. 194 (2013) http://dx.doi.org/10.1016/j.jnnfm.2012.10.007.